Applied Mathematical Modelling 37 (2013) 4809–4824

Contents lists available at SciVerse ScienceDirect

Applied Mathematical Modelling

journal homepage: www.elsevier.com/locate/apm

Existence and numerical modelling of vortex rings with elliptic boundaries

Yan Zhang *, Ionut Danaila

UPMC Univ Paris 06, UMR 7598, Laboratoire Jacques-Louis Lions, F-75005 Paris, France
Laboratoire de Mathématiques Raphaël Salem, Université de Rouen, F-76801 Saint-Étienne-du-Rouvray, France

ARTICLE INFO

Article history:
Received 6 June 2012
Received in revised form 10 September 2012
Accepted 1 October 2012
Available online 16 October 2012

Keywords:
Vortex rings
Elliptic operator
Finite element method

ABSTRACT

We revisit in this paper the theory of axisymmetric vortex rings in an ideal fluid. The boundary separating the vortex ring from the external (potential) flow is assumed of elliptic shape. For a given distribution of vorticity in the vortex core, we theoretically put into evidence the critical parameter for the existence of non-trivial solutions, thus confirming the numerical observation of Durst et al. [ZAMP 32 (1981) 156]. A sharp estimation of the critical threshold is analytically derived. Theoretical predictions are confirmed by numerical simulations using finite elements. A new numerical algorithm is presented and shown to display better performances compared to previous published algorithms using finite differences. The convergence of the iterative algorithm is proved using the theory of elliptic partial differential equations with discontinuous nonlinearities.

© 2012 Elsevier Inc. All rights reserved.

1. Introduction

Vortex rings appear as coherent fluid structures in numerous application fields, ranging from bio-mechanics (e.g. the blood entry in the left ventricle during cardiac diastole, or the propulsion of squid or jellyfish) to engineering situations (e.g. injection in internal combustion engines, or actuation mechanisms using synthetic jets). This explains a renewal of the interest in studying mathematical and physical properties of vortex rings. In particular, analytical vortex ring models have been recently used to predict the evolution of complicated flows and realize diagnosis of practical interest, as, for example, in describing biological propulsion [1,2] or in analyzing the fuel injection in automobile engines [3,4].

The evolution of vortex ring flows was recently studied in [5] by numerically solving the governing incompressible Navier–Stokes equations. Numerical results were compared to ideal vortex models of Norbury and Fraenkel [6,7] and Kaplanski and Rudi [8] and showed fairly good agreement. This enforces the idea of using such simplified mathematical models in studying complicated flows encountered in physical applications.

In this paper, we revisit some mathematical results of the theory of axisymmetric vortex rings developed in the 70s and early 80s, and bring new theoretical and numerical contributions aimed at improving the use of vortex ring models for practical applications. We consider the particular problem when the boundary separating the vortex ring from the external (potential) flow has a particular elliptic shape, which is relevant for real vortex ring flows. This problem was first studied by Durst et al. [9,10], who numerically investigated the characteristics of such elliptic vortex rings and pointed out some interesting theoretical questions that have since remained unanswered. In particular, no theoretical justification was provided to explain the numerical evidence that non-zero solutions exists only for a limited domain in the space of parameters. Also, the convergence of the iterative algorithm used to compute the solution was not presented. This is a delicate question, since the vortex ring problem is described by a non-linear partial differential equation with a discontinuous source term and standard analysis cannot be applied.

* Corresponding author at: UPMC Univ Paris 06, UMR 7598, Laboratoire Jacques-Louis Lions, F-75005 Paris, France.
E-mail address: yanzhxj@gmail.com (Y. Zhang).

0307-904X/$ - see front matter © 2012 Elsevier Inc. All rights reserved.
http://dx.doi.org/10.1016/j.apm.2012.10.013

In order to answer these open questions, the present paper brings the following new contributions: (i) we theoretically put into evidence the critical parameter for the existence of non-trivial solutions and give an estimation of its limiting value; we derive a sharp estimation that matches numerical results and, therefore, could be used for practical applications; (ii) we design an efficient numerical algorithm to compute vortex ring solutions that is faster than existing methods; we theoretically prove its convergence for discontinuous parameters of the model, and emphasize the practical implications of this analysis.

The paper is organized as follows. In the remaining of the introductory part, we describe the general problem of the inviscid vortex ring model and the particular formulation for the elliptic vortex ring. A first theoretical part presents two different estimations for the limiting value of the parameters for which non-trivial solutions exist. The first estimation uses the first eigenvalue of the elliptic operator; a second, sharper estimation also involves results on the capacity of the elliptic operator. The second theoretical part develops the numerical algorithm based on monotone iterations. The convergence of the algorithm is proved in the general framework of elliptic partial differential equations with discontinuous nonlinearities. We prove the convergence of the algorithm when finite elements are used for the spatial discretization. Theoretical estimations are compared to numerical results in the final part, which also discusses the efficiency of the algorithm and practical implications of theoretical results.

1.1. Mathematical formulation of the general problem

The flow being axisymmetric, we use cylindrical coordinates to describe it, with (z, r, θ) denoting the longitudinal, radial and azimuthal direction of the flow, respectively. We also consider that the motion is steady in a reference frame translating with the vortex ring translation velocity W (assumed constant). Let ψ denote the Stokes stream function in this reference frame. The advantage of this description is that inside the vortex ring the fluid circulates over closed streamlines $\psi = const.$, while the streamlines are open for the external flow (see Fig. 1a). Following Fig. 1b, the vortex bubble Ω_b is defined by the dividing streamline ($\psi = 0$) and the forward (A) and, respectively, rearward (B) stagnation points. The flow outside the vortex bubble is considered as a potential flow. The vorticity is concentrated in the vortex core Ω_c and is zero elsewhere. It is generally assumed that the vortex core boundary $\partial\Omega_c$ is a streamline $\psi = k$, with k a positive constant. Physically, $2\pi k$ represents the flow rate between the axis $0z$ and $\partial\Omega_c$. On the axis of symmetry ($r = 0$) the radial velocity is $v_r = 0$ and, consequently, $\psi = 0$.

The axial-symmetry of the flow allows to define the problem on the half-plane $\Pi = \{(z, r)|r > 0\}$. Using the notations indicated in Fig. 1b, the problem of the inviscid, steady vortex ring can be stated as follows: given two positive constants, W (the translation velocity) and k (the flux constant) and given the (vorticity) function f, find the stream function ψ and the boundary $\partial\Omega_c$ of the vortex core such that

$$\mathcal{L}\psi = \begin{cases} rf(\psi + \frac{1}{2}Wr^2), & \text{in} \quad \Omega_c \\ 0, & \text{in} \quad \Pi \setminus \bar{\Omega}_c, \end{cases} \tag{1}$$

where $\mathcal{L}$ is the self-adjoint elliptic operator given by:

$$\mathcal{L} = -\left(\frac{\partial}{\partial z}\left(\frac{1}{r}\frac{\partial}{\partial z}\right) + \frac{\partial}{\partial r}\left(\frac{1}{r}\frac{\partial}{\partial r}\right)\right) = -\nabla \cdot \left(\frac{1}{r}\nabla\right), \tag{2}$$

with $\nabla = \left(\frac{\partial}{\partial z}, \frac{\partial}{\partial r}\right)^t$. We note that $\mathcal{L}(\frac{1}{2}Wr^2 + k) = 0$, with W and k real constants.

The additional constraints on the solution are:

$$\psi \text{ and } \nabla\psi \text{ are continuous across } \partial\Omega_c, \tag{3}$$

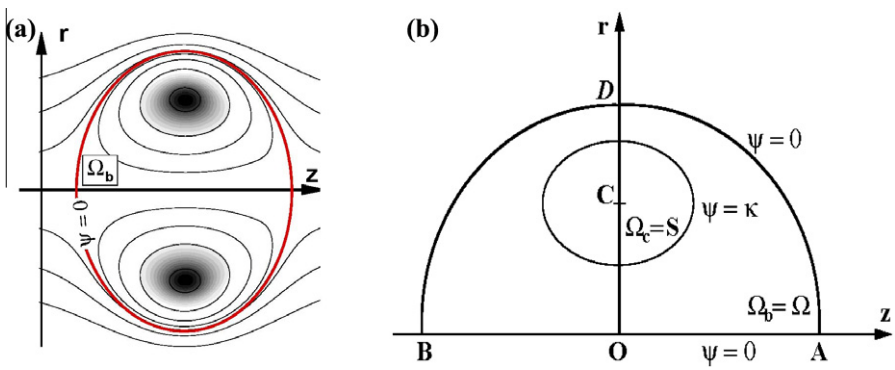

Fig. 1. (a) Physical vortex ring reproduced by direct numerical simulation of the incompressible Navier–Stokes equations [5]. Streamlines in the frame of reference travelling with the vortex ring velocity. Gray region represents vorticity. (b) Domain definition for the vortex ring problem.

$$\psi = k \text{ on } \partial\Omega_c, \quad \psi = 0 \text{ on } Oz, \tag{4}$$

$$\psi + \frac{1}{2}Wr^2 \to 0 \text{ when } r^2 + z^2 \to \infty. \tag{5}$$

An additional constraint could be imposed [11,12] by prescribing the kinetic energy of the vortex ring:

$$\eta = \int_\Pi (v_r^2 + v_z^2) r dr dz = \int_\Pi \frac{1}{r} |\nabla\psi|^2 dr dz. \tag{6}$$

If $\eta > 0$ is imposed as normalization condition of the solution, trivial solutions are excluded. For this new problem, global existence of solutions was first proved in the comprehensive study by Fraenkel and Berger [11].

The main difficulty in solving the vortex ring problem comes from the fact that the boundary $\partial\Omega_c$ is not known, which makes it a *free boundary problem*. The problem could be reduced to a semi-linear elliptic problem [11] by extending f as:

$$f(r,\psi) > 0, \quad \forall\psi > k, \quad \text{and} \quad f(r,\psi) = 0, \quad \forall\psi \leqslant k. \tag{7}$$

It results, by the maximum principle, that the vortex core Ω_c could be defined as:

$$\Omega_c = \{\mathbf{x} \in \Pi; \psi(\mathbf{x}) \geqslant k\}, \tag{8}$$

and Eq. (1) is equivalent to:

$$\mathcal{L}\psi = rf\left(r, \psi + \frac{1}{2}Wr^2\right), \quad \text{in} \quad \Pi. \tag{9}$$

The problem described by (9) with constraints (3)–(5) is also called the *free energy problem*. We shall address in the following the free energy problem that allows to fix W and k and search for a solution of (9) with non-zero energy.

A different reformulation of the problem, as a semi-linear Dirichlet boundary value problem for the Laplacian in cylindrical coordinates in $\mathbb{R}^5$, was introduced in [13]. This made possible the use of variational techniques to prove existence results [13,14], symmetry [15] or asymptotic behavior [16] of solutions.

From a practical point of view, the expression of the vorticity function f will define a *vortex ring model*. We shall consider in this paper the Norbury–Fraenkel model [7,6], that is nowadays largely used to describe real vortex rings generated experimentally [2] or numerically [5,17]. The model assumes that $f|_{\Omega_c} = C$, with C a positive constant, also called the *vortex strength*. The limiting case with $k = 0$ corresponds to a vortex core occupying the entire vortex bubble, i.e. $\Omega_c = \Omega_b$; when Ω_c is a sphere, we obtain the Hill's spherical vortex [18–20]. It is easy to notice that in this case, the Eq. (9) becomes a nonlinear eigenvalue problem.

Existence and uniqueness results for this problem are presented in [11,21] for the general case and in [22,23] for vortex rings bifurcating from Hill's vortex. Numerical computations of such solutions are presented in [6] using finite difference methods and in [12] using an adaptive finite element method.

1.2. Problem of the vortex ring with elliptic boundary

A further simplification of the free energy vortex problem is obtained if the boundary $\Gamma_b = \partial\Omega_b$ of the vortex bubble is fixed. In the following, we consider elliptic shapes that reasonably match real vortex rings. Since $\Gamma_c = \partial\Omega_c$ depends on the solution ψ, known to be monotonic [11], the problem can be formulated as follows (see Fig. 1b): for a given vortex strength $C > 0$ and flux constant $k \geqslant 0$, find the stream function ψ such as:

$$\mathcal{L}\psi = rCI_{\psi \geqslant k} = \begin{cases} rC, & \text{if} \quad \psi \geqslant k \\ 0, & \text{otherwise}, \end{cases} \tag{10}$$

where the characteristic function I identifies now the vortex core Ω_c defined by (8). The boundary condition is a homogeneous Dirichlet condition $\psi = 0$ on $\Gamma_b = \partial\Omega_b$. Since it is convenient to use scaled space coordinates, the boundary Γ_b will be described in the following by $r^2 + (z/\alpha)^2 = 1$, where $\alpha \leqslant 1$ denotes the minor half-axis of the ellipse ($|OD| = 1, |OA| = \alpha$ in Fig. 1b.

It is interesting to note that prescribing the boundary of the vortex bubble, it is equivalent to fix the velocity W of the flow at infinity. We recall that the external flow is defined as the potential flow over the ellipsoid obstacle defined by the vortex ring bubble. As a consequence, the two remaining parameters of the problem are C and k.

Existence results of solutions of the vortex ring problem on a bounded domain Ω are discussed in [12] for a general class of vorticity functions f. Durst et al. [9,10] investigated this problem numerically by a finite difference method using elliptic coordinates. They searched nonzero solutions for two distinct problems of physical interest:

(i) for a fixed value of C, find admissible values $0 \leqslant k \leqslant k_{max}$ such as that $\psi \neq 0$, which physically means that a vortex of a given strength needs a minimum vortex core area to exist;

(ii) for a fixed value of k, find admissible values $C > C_{min}$; in other terms, find the minimum vortex strength needed for a vortex to exist when the flow rate is given.

Durst et al. finally summarized their numerical findings in the following conjecture:

Conjecture 1. The problem (10) of the vortex ring with elliptic boundary admits nonzero solutions if

$$0 \leqslant \delta = \frac{k}{C} \leqslant \delta_{max} \quad \Longleftrightarrow \quad \delta^{-1} \geqslant 1/\delta_{max}. \tag{11}$$

The purpose of the present contribution is therefore twofold: (i) to theoretically demonstrate this conjecture and give an estimation of the critical value δ_{max}, and (ii) to propose a new, more efficient algorithm, to compute vortex rings with elliptic boundaries and theoretically prove its convergence.

2. Theoretical analysis and estimation of critical parameters

An easy way to put into evidence the parameter δ defined by (11) is to rescale the initial problem (10) by defining the variable $\widehat{\psi} = \frac{\psi}{C}$. We obtain the following equivalent problem:

$$\mathcal{L}\widehat{\psi} = rI_{\widehat{\psi} \geqslant k/C = \delta}. \tag{12}$$

For the sake of simplicity, we drop the $\widehat{()}$ notation; in the following, all variables will refer to the scaled problem (12). It is also convenient to consider in this part the problem (12) defined on the whole domain Ω_b (see Fig. 1b) in order to set homogeneous Dirichlet boundary conditions ($\psi = 0$) on all boundaries.

To illustrate the conjecture we intend to prove, we show in Fig. 2 several solutions numerically computed for the same elliptic boundary $\alpha = 0.6$ and different values $0 \leqslant \delta \leqslant \delta_{max}$. For $\delta > \delta_{max}$ the numerical solution goes to the trivial $\psi = 0$ solution.

We give in the following sections two estimations of the critical value δ_{max} which condition the existence of nonzero solutions.

2.1. Preliminaries

Following [11,12], let us denote $\Omega \equiv \Omega_b$ (the vortex bubble), $S \equiv \Omega_c$ (the vortex core) and introduce the function space:

$$H_0(\Omega) = \left\{ u \in L^2(\Omega); \frac{1}{r}|\nabla u|^2 \in L^1(\Omega) | u = 0 \quad \text{on} \quad \Gamma = \partial\Omega \right\}. \tag{13}$$

$H_0(\Omega)$ is the closure of the standard test functions space for the Hilbert norm:

$$\|u\|_{H_0(\Omega)} = \left(\int_\Omega |u|^2 d\tau + \int_\Omega \frac{1}{r^2} |\nabla u|^2 d\tau \right)^{1/2}, \quad d\tau = rdrdz. \tag{14}$$

It is interesting to note that the seminorm

$$\|u\| = \left(\int_\Omega \frac{1}{r^2} |\nabla u|^2 d\tau \right)^{1/2} = \left(\int_\Omega \frac{1}{r} |\nabla u|^2 dx \right)^{1/2}, \quad dx = drdz, \tag{15}$$

is in fact a norm on $H_0(\Omega)$, equivalent to the norm (14) (see [11,12]), and hence

$$a(u, v) = \int_\Omega \frac{1}{r} \nabla u \nabla v \, dx, \tag{16}$$

is an $H_0(\Omega)$ elliptic symmetric bilinear form corresponding to the inner product $\langle u, v \rangle = a(u, v)$.

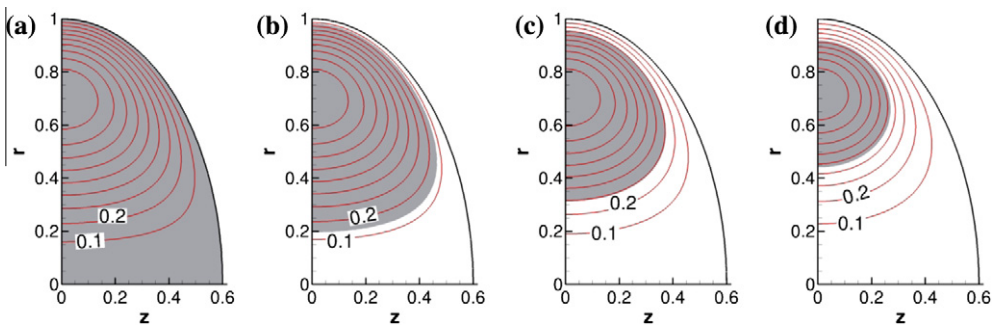

Fig. 2. Solutions for the elliptic vortex with $\alpha = 0.6$. Isolines of ψ/ψ_{max} for (a) $\delta = 0$, (b) $\delta^{-1} = 400$, (c) $\delta^{-1} = 200$, (d) $\delta^{-1} = 154$. The critical value for this case is $\delta_{max} = 1/153.28$. Gray zones correspond to vortex cores ($\psi > \delta$).

We notice, in passing, that the norm (15) has a physical signification since it represents the kinetic energy (6) of the vortex ring ($\eta = \|u\|^2$). We consider in the following the space $H_0(\Omega)$ equipped with the inner product inducing the norm (15); this a natural setting for the problem (12), since

$$\langle u, v\rangle = \int_\Omega \frac{1}{r}\nabla u \nabla v\, dx = \int_\Omega u\mathcal{L}v\, dx, \quad \text{for} \quad u \in H_0(\Omega), v \in H_0(\Omega) \cap C^2(\overline{\Omega}). \tag{17}$$

We also consider the eigenvalue problem associated to the operator $\mathcal{L}$ under the form: find $\lambda \in \mathbb{R}$ and $u \in H_0(\Omega)$ such that

$$a(u, v) = \lambda(u, v), \quad \forall v \in H_0(\Omega), \tag{18}$$

where (u, v) denotes the $L^2(\Omega)$ inner product. We define the first eigenvalue by

$$\lambda_1 = \inf_{u \in H_0(\Omega), u \neq 0} \frac{a(u, u)}{(u, u)}. \tag{19}$$

Since $a(u, v)$ is an elliptic symmetric bilinear form and positive, $\lambda_1 > 0$ exists and is finite.

Finally, we recall the definition of the (electrostatic) capacity relative to an elliptic operator $\mathcal{L}$. Let S be a compact subset of Ω, the capacity of S in Ω is generally defined [24,16,25] as:

$$\mathrm{Cap}_{\mathcal{L}}(S, \Omega) = \inf\left\{\int_{\Omega\setminus\overline{S}} u\mathcal{L}u | u \in H_{\mathcal{L}}, u|_E \geqslant 1\right\}, \tag{20}$$

where $H_{\mathcal{L}}$ is the Hilbert space equipped with the norm $\|u\| = \int_\Omega u\mathcal{L}u$ and $u|_S \geqslant 1$ means that there is a sequence in $H_{\mathcal{L}}$ such that $u_n \geqslant 1$ on S for each n and $\|u - u_n\| \to 0$ when $n \to \infty$.

In the case of the Laplace operator $\mathcal{L} = -\Delta$, in two dimensions denoted by (r, z), the function space $H_{\mathcal{L}}$ is the Sobolev space

$$W_0^{1,2}(\Omega) = \left\{u \in H^1(\Omega) | u = 0 \quad \text{on} \quad \Gamma = \partial\Omega\right\}. \tag{21}$$

with the norm $\|u\|_{1,2} = \left(\int_\Omega |\nabla u|^2\right)^{1/2}$. It is easy to see from definitions (13) and (15) that $H_0(\Omega)$ is embedded in $W_0^{1,2}(\Omega)$ (see also [16]), since for $\psi \in H_0(\Omega)$ we can write that:

$$\|u\|_{1,2} \leqslant \|r\|_{L^\infty(\Omega)}\|u\|. \tag{22}$$

The case of the Laplace operator is interesting since a sharp estimation of the capacity is provided in [26]:

$$\mathrm{Cap}_{-\Delta}(S, \Omega) \geqslant G(\varepsilon), \tag{23}$$

where

$$G(\varepsilon) = \frac{8K(\varepsilon^2)}{K([1 - \varepsilon^4]^{1/2})}, \quad \varepsilon = \frac{\mathrm{diam}(S)}{\mathrm{diam}(\Omega)}, \tag{24}$$

and

$$K(\varepsilon) = \int_0^1 \left\{(1 - t^2)(1 - \varepsilon^2 t^2)\right\}^{-1/2} \mathrm{d}t, \quad 0 \leqslant \varepsilon < 1. \tag{25}$$

The expression of the integral (24) is:

$$G(\varepsilon) = \frac{8\sqrt{1 - \varepsilon^4}\,\mathrm{EllF}(\varepsilon^2, 1/\varepsilon^2)}{\varepsilon^2 \mathrm{EllF}\left(\sqrt{1 - \varepsilon^4}, 1/\sqrt{1 - \varepsilon^4}\right)}, \tag{26}$$

where $\mathrm{EllF}(\cdot, \cdot)$ denotes the incomplete elliptic integral of the first kind.

2.2. Estimations of the critical parameter

A first rapid estimation of the critical parameter δ_{max} could be obtained directly using the first eigenvalue solely. This idea was suggested to us by Le [27] (see also [28]) and results in the following proposition:

Proposition 1. *Nonzero solutions of the problem (12) exist if*

$$0 \leqslant \delta \leqslant \frac{1}{\lambda_1} \iff \delta^{-1} \geqslant \lambda_1, \tag{27}$$

where λ_1 is the first eigenvalue of the operator $\mathcal{L}$ on Ω.

Proof. Let $\lambda_1 > 0$ be the first eigenvalue of $\mathcal{L}$ on Ω, defined by (19). We can choose an associated eigenfunction φ such that φ is positive in Ω.

Multiplying both sides of (12) by φ we obtain:

$$\int_\Omega r I_{\{\psi \geqslant \delta\}} \varphi \, dx = \int_\Omega \varphi \mathcal{L} \psi \, dx = a(\psi, \varphi) = \lambda_1 \int_\Omega \psi \varphi \, dx. \tag{28}$$

It follows that:

$$\|r\|_\infty \int_{\{\psi \geqslant \delta\}} \varphi \, dx \geqslant \lambda_1 \int_\Omega \psi \varphi \, dx \geqslant \lambda_1 \int_{\{\psi \geqslant \delta\}} \psi \varphi \, dx \geqslant \delta \lambda_1 \int_{\{\psi \geqslant \delta\}} \varphi \, dx. \tag{29}$$

Because ψ is not trivial, we have that $\int_{\{\psi \geqslant \delta\}} \varphi > 0$ and from the previous inequality we deduce, since $\|r\|_\infty = 1$ in our setting, that

$$\delta \leqslant \frac{1}{\lambda_1}. \tag{30}$$

This first estimation is not very sharp, as shown in Fig. 3, displaying the limiting curve for δ_{max} (in order to compare with the results of Durst et al. [9,10], we plot δ^{-1}). Numerical values for the problem (12) are computed using the method described in the next section. Eigenvalues and eigenvectors are computed using the shift–invert mode method implemented in ARPACK library.

A second, sharper estimation of the critical parameter is thus derived using jointly the first eigenvalue and the capacity of the elliptic operator.

Proposition 2. *Nonzero solutions of the problem (12) exist if*

$$\delta^{-1} \geqslant 3.73642\lambda_1 - \frac{0.990004\sqrt{G(\varepsilon)\lambda_1}}{\sqrt{\alpha}} \pm \frac{\sqrt{0.980108\, G(\varepsilon)\lambda_1 - 7.39814\lambda_1^{3/2}\sqrt{G(\varepsilon)\alpha} + 7.84451\lambda_1^2\alpha}}{\sqrt{\alpha}}. \tag{31}$$

where α is the geometric parameter of the ellipse, and G is given by (24). This estimation is based on the following geometrical approximations:

$$r_c \simeq 1/\sqrt{2}, \quad \varepsilon \sim \frac{\sqrt{2}\alpha}{1+\alpha^2}. \tag{32}$$

Proof. We start by relating the energy η to the capacity of the Laplacian. From definitions (6) and (15), we get:

$$\eta = \|\psi\|^2 = \int_\Omega \frac{1}{r}|\nabla\psi|^2 \, dx \geqslant \frac{\delta^2}{\|r\|_\infty} \int_\Omega \left|\nabla\left(\frac{\psi}{\delta}\right)\right|^2 dx \geqslant \delta^2 \int_S \left|\nabla\left(\frac{\psi}{\delta}\right)\right|^2 dx, \tag{33}$$

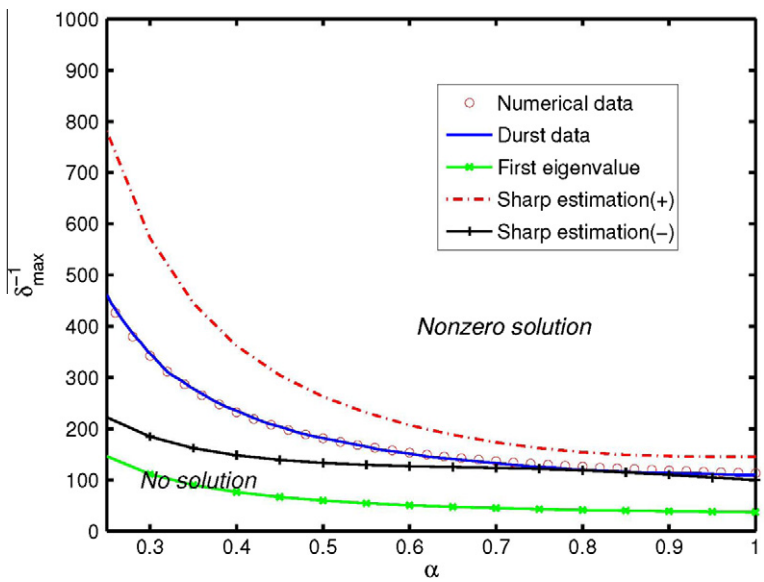

Fig. 3. Plot of the limiting curve for the critical parameter δ_{max}. Nonzero solutions exist for $\delta^{-1} > 1/\delta_{max}$. Comparison between present numerical results, the results of Durst et al. [9,10] and our theoretical sharp estimations denoted by "+" and " −".

since $\|r\|_\infty = 1$ in our setting, and $S \subseteq \Omega$. We can use now (24) to obtain:

$$\eta \geqslant \delta^2 \operatorname{Cap}_{-\Delta}(S,\Omega) \geqslant \delta^2 G(\varepsilon). \tag{34}$$

In the same time, we can write from (15) and (17) that

$$\eta = \|\psi\|^2 = \int_\Omega \psi \mathcal{L}\psi \, dx = \int_\Omega \psi r I_{\psi \geqslant \delta} \, dx = \int_S \psi r \, dx, \tag{35}$$

and, by Cauchy–Schwarz we obtain the inequality:

$$\eta \leqslant \left(\int_S r^2 \right)^{1/2} \|\psi\|_{L^2(S)}. \tag{36}$$

The above integral could be expressed by using the generalized Lagrange mean value theorem as follows:

$$\eta \leqslant r_c |S|^{1/2} \|\psi\|_{L^2(S)}, \qquad r_c \in S. \tag{37}$$

Since from the definition (19) of the first eigenvalue of the operator L, we have $\|\psi\|^2_{L^2(S)} \leqslant \eta/\lambda_1$. Then, we have:

$$\eta^{1/2} \leqslant r_c |S|^{1/2} \lambda_1^{-1/2}. \tag{38}$$

Combining this inequality with (34), we finally obtain that:

$$\delta^{-1} \geqslant \frac{(G(\varepsilon)\lambda_1)^{1/2}}{r_c |S|^{1/2}}. \tag{39}$$

We need now to get into more detail concerning the geometry of the vortex ring. Assuming that $r_c \simeq 1/\sqrt{2}$, which is the center of the Hill's spherical vortex (see [9,10] and the next section), a rough estimation of the area $|S|$ of the vortex core is (we consider as upper bound the part of the ellipse above the line $r = 2r_c - 1$):

$$|S| \leqslant 2\left(\frac{1}{4}\pi\alpha - \frac{1}{2}\sqrt{1-(2r_c-1)^2}(2r_c-1)\alpha - \frac{1}{2}\alpha \operatorname{ArcSin}(2r_c-1) \right). \tag{40}$$

Follow the same assumption on the value of r_c, we use a Taylor expansion at $1/\sqrt{2}$ and estimate by a second-order approximation:

$$r_c |S|^{1/2} \leqslant 0.619156\sqrt{\alpha} - 0.594413\sqrt{\alpha}(r_c - 1/\sqrt{2}) - 3.08904\sqrt{\alpha}(r_c - 1/\sqrt{2})^2 + O\left((r_c - 1/\sqrt{2})^3\right). \tag{41}$$

Meanwhile, from the Eq. (35), we have:

$$\eta = \int_S \psi r dx \geqslant \delta \int_S r dx. \tag{42}$$

Combining this equation with (38), we obtain that:

$$\delta \int_S r dx \leqslant \eta \leqslant r_c^2 |S| \lambda_1^{-1} \tag{43}$$

and, using the definition of $r_c = \left(\int_S r^2 dx/|S|\right)^{1/2}$,

$$r_c^2 \geqslant \delta\lambda_1 \left(\frac{\int_S r dx}{|S|} \right) \geqslant \delta\lambda_1 r_c. \tag{44}$$

Finally, we obtain a lower bound for r_c, that could also be used as a better estimation of the critical parameter than (27):

$$r_c \geqslant \delta\lambda_1. \tag{45}$$

It is easy to see from (41) that the function $G(r_c) = r_c |S(r_c)|^{1/2}$ is decreasing. As a consequence $G(r_c) \leqslant G(\delta\lambda_1)$ and from (39) we infer that:

$$\delta^{-1} \geqslant \sqrt{G(\varepsilon)}\lambda_1^{1/2} / \left(0.619156\sqrt{\alpha} - 0.594413\sqrt{\alpha}(\delta\lambda_1 - 1/\sqrt{2}) - 3.08904\sqrt{\alpha}(\delta\lambda_1 - 1/\sqrt{2})^2\right). \tag{46}$$

The limiting curve of this implicit relationship is exactly the right-hand side of the inequality (31) (the coefficients are calculated using Mathematica).

Finally, we give a rough estimation of ε. The circumscribed circle diameter of the domain Ω is equal to $1+\alpha^2$, and $\operatorname{Diam}(S) \sim \sqrt{2}v$, resulting in the estimation:

$$\varepsilon = \frac{\operatorname{Diam}(S)}{\operatorname{Diam}(\Omega)} \sim \frac{\sqrt{2}\alpha}{1+\alpha^2}. \tag{47}$$

The two limiting curves given by (31) are also represented in Fig. 3. This second estimation, that includes a rough representation of the geometry of the vortex and the classical estimation of the capacity of the elliptic operator, is obviously sharper than the first estimation based solely on the first eigenvalue of the operator. From a practical point of view, the second estimation (+) offers a good starting point if one intends to explore admissible nonzero vortex ring solutions in a given domain of elliptic shape. This situation is encountered in practical applications, as discussed in the final part of this paper. This sharp theoretical estimation of the critical parameter is also important to increase the convergence of computations searching numerically for the critical value δ_{max} (as stated in the section presenting numerical results).

3. Numerical algorithm and finite element method

The problem (12) is numerically solved using finite elements methods. We start by presenting the numerical algorithm and analyze its convergence in the case of discontinuous data. Then we prove convergence of the finite element method. For the numerical implementation, we use the free software FreeFem++ [29] using a large variety of triangular finite elements to solve partial differential equations in two or three dimensions. FreeFem++ is an integrated product with its own high level programming language with a syntax close to mathematical formulations; it was recently used to test algorithms for the minimization of Schrödinger or Gross-Pitaevskii functionals [30,31].

3.1. A monotone iterative algorithm

We consider the scaled problem (12) defined on the entire domain depicted in Fig. 1b. The variational formulation of (12) is given as follows:

Find $\psi \in H_0(\Omega)$, such that:

$$a(\psi, \phi) = l(\phi), \quad \forall \phi \in H_0(\Omega), \tag{48}$$

where the bilinear form $a(u, v)$ is given by (16) and

$$l(v) = (F, v) = \int_\Omega F v \, dx, \quad F = r I_{\psi \geqslant \delta}. \tag{49}$$

Note that this problem is defined with homogeneous Dirichlet boundary conditions. For numerical calculations we can use the symmetry of the solution [11,15] with respect to the Or axis, and consider the problem only on a half-domain ($z > 0$), with a symmetry Neumann boundary condition $\frac{\partial \psi}{\partial z}(r, z) = 0$ on $\Gamma_r = OD$.

Numerical methods for solving the problem of vortex rings generally use [12,6] monotone iterations to converge to the final shape of the vortex ring core $\Omega_c = \{x \in \Omega : \psi \geqslant \delta\}$. In our case, the right-hand side of (12) is a discontinuous Heaviside function, and, therefore, we have to take care in deriving the numerical algorithm of the fact that the problem (12) is multivalued [32–35]. This means that, if we take two special initial conditions, two different convergent solutions will be obtained by a monotone iteration algorithm. The proof of the convergence of our algorithm will use the framework developed in [34,32,36,37] for monotone iterations of elliptic partial differential equations with discontinuous nonlinearities. We start with some definitions.

Definition 1. A function $\psi \in H_0(\Omega)$ is said to be an upper solution of (12), if the following condition is satisfied

$$a(\psi, \phi) \geqslant l(\phi), \quad \forall \phi \in H_0(\Omega), \quad \phi \geqslant 0. \tag{50}$$

A lower solution is defined similarly by reversing the sign of the above inequality [34,32]. An element $\psi \in H_0(\Omega)$ is a solution of (48) if and only if it forms simultaneously an upper and a lower solution. In the following, we study the convergence of the algorithm for a given value δ. The existence of vortex ring solutions of nonzero energy in a bounded domain was proved in [12] using the Shauder's fixed point theorem for a more general function F. It is thus reasonable to suppose that:

Assumption 1. There exist ψ_l^0 (a lower solution) and ψ_u^0 (an upper solution) such that the following condition is satisfied

$$0 \leqslant \psi_l^0 \leqslant \psi_u^0, \quad \text{a.e.}, \quad \forall x \in \Omega, \tag{51}$$

where a partial ordering in the spaces $L^2(\Omega), H_0(\Omega)$ was introduced by $u \leqslant v$ if and only if $v - u$ belongs to the set $L^2_+(\Omega)$ of all nonnegative elements of $L^2(\Omega)$.

We also define the following sets for any $\delta^* \leqslant \delta_{max}$:

$$\Omega_{\delta^*}(\psi) = \{x \in \Omega \,|\, \psi \geqslant \delta^*\}, \quad \Gamma_{\delta^*}(\psi) = \{x \in \Omega \,|\, \psi = \delta^*\}. \tag{52}$$

The iteration algorithm is defined [34] separately for the lower solution:

$$(\text{init})\, \psi_l^0; \quad (\text{solve})\, a(\psi_l^n, \phi) = \left(F(\psi_l^{n-1}), \phi\right), \quad \forall \phi \in H_0(\Omega),\ \phi > 0 \tag{53}$$

and for the upper solution:

$$(\text{init})\, \psi_u^0; \quad (\text{solve})\, a(\psi_u^n, \phi) = \left(F(\psi_u^{n-1}), \phi\right), \quad \forall \phi \in H_0^1(\Omega),\ \phi > 0. \tag{54}$$

Because $\psi_l^n, \psi_u^n \in H_0^1(\Omega)$ are monotone increasing and monotone decreasing sequences respectively (see also [12]), we can define the following ordered sets for a specified $\delta^* \leqslant \delta_{max}$

$$\Omega_{\delta^*}(\psi_l^{n-1}) \subset \Omega_{\delta^*}(\psi_l^n), \tag{55}$$

and

$$\Omega_{\delta^*}(\psi_u^n) \subset \Omega_{\delta^*}(\psi_u^{n-1}). \tag{56}$$

When the iteration process is convergent, the ordered set $\Omega_{\delta^*}(\psi_u^n)$ converge to the vortex core Ω_δ. The following theorem gives the convergence of the algorithms.

Theorem 1. *Under Assumption 1, the iterations schemes guarantee the following bounds*

$$\psi_l^n \leqslant \psi_l^{n+1} \leqslant \cdots \leqslant \psi_u^{n+1} \leqslant \psi_u^n. \tag{57}$$

Also, there exist convergent solutions ψ_l^* and ψ_u^* for the iteration algorithm (53) and (54) respectively, within the interval $[\psi_l^0, \psi_u^0]$.

Proof. First, we show that the obtained sequence ψ_l^n is non-decreasing. Let us assume that $\psi_l^{n-1} \leqslant \psi_l^n$; because $F(\cdot)$ is a non-decreasing function, we have

$$(F(\psi_l^n), \phi) - (F(\psi_l^{n-1}), \phi) \geqslant 0. \tag{58}$$

That means that

$$a(\psi_l^{n+1}, \phi) \geqslant a(\psi_l^n, \phi). \tag{59}$$

and

$$a(\psi_l^{n+1} - \psi_l^n, \phi) \geqslant 0. \tag{60}$$

Since $a(u, v)$ is a bilinear symmetric form, by the strong maximum principle [38] and the zero boundary conditions, we have

$$\psi_l^{n+1} \geqslant \psi_l^n. \tag{61}$$

The same reasoning applies for the first iteration. It is known that for any $\phi \in H_0^1(\Omega)$ $(\phi > 0)$

$$a(\psi_l^0, \phi) \leqslant (F(\psi_l^0), \phi), \tag{62}$$

and

$$a(\psi_l^1, \phi) = (F(\psi_l^0), \phi). \tag{63}$$

From the above, we infer that $\psi_l^0 \leqslant \psi_l^1$, which ends the first part of the proof concerning ψ_l.

The similar result $\psi_u^{n+1} \leqslant \psi_u^n$ can be obtained in the same way. By Assumption 1, it is clear that $\psi_l^0 \leqslant \psi_u^0$. If we assume $\psi_l^n \leqslant \psi_u^n$, by a similar argument, we have

$$\psi_l^{n+1} \leqslant \psi_u^{n+1}. \tag{64}$$

and the relation (57) is satisfied.

Finally, we show convergence properties for ψ_l^{n+1}. Starting from (22), we derive the following inequality:

$$\|\nabla \psi_l^{n+1}\|_{L^2(\Omega)}^2 \leqslant a\left(\psi_l^{n+1}, \psi_l^{n+1}\right) = \left(F(\psi_l^n), \psi_l^n\right) \leqslant \|F(\psi_l^n)\|_{L^2(\Omega)} \|\psi_l^n\|_{L^2(\Omega)}. \tag{65}$$

Since $\{\psi_l^n\}$ is uniformly bounded in $L^2(\Omega)$, by (65), $\{\psi_l^n\}$ is uniformly bounded in $H_0^1(\Omega)$. Because the embedding $H_0^1(\Omega) \hookrightarrow L^2(\Omega)$ is compact [39], a subsequence $\{\psi_l^{n_i}\}$ can be extracted which converges to ψ_l^* weakly in H_0^1 and strongly in $L^2(\Omega)$.

It is clear that $\psi_l^n \leqslant \psi_l^* \in [\psi_l^0, \psi_u^0]$ for any $n \in \mathbb{Z}^+$, since the whole sequence $\{\psi_l^n\}$ is partial ordered and $\lim_{n \to \infty} \psi_l^n = \psi_l^*$. Because $\psi_l^* \geqslant \psi_l^n$ for any $n \in \mathbb{Z}^+, a(\psi_l^*, \phi) \geqslant (F(\psi_l^n), \phi)$. Meanwhile, $a(\psi_l^*, \phi) \leqslant (F(\psi_l^*), \phi)$, so the convergence limit ψ_l^* is a lower solution of (12).

The similar result can be obtained for the upper solution. □

3.2. Finite element approximation

We outline here the main features of the finite element implementation which follows standard methods. Let $\mathcal{T}_h$ be a family of triangulations of the domain Ω. We assume that $\mathcal{T}_h$ is a regular family in the sense of Ciarlet [40], with $h > 0$ belonging to a generalized sequence converging to zero. We denote by $P^l(T)$ the space of polynomial functions on triangles $T \in \mathcal{T}_h$, of degree not exceeding $l \geqslant 1$. We also introduce the finite element approximation spaces:

$$W_h^l = \left\{ w_h \in C^0(\bar{\Omega}_h); w_h|_T \in P^l(T), \forall T \in \mathcal{T}_h \right\}, \tag{66}$$

and

$$V_h^l = \left\{ w_h \in W_h^l; w_h|_{\Gamma_h} = 0 \right\}. \tag{67}$$

The finite dimensional space V_h^l is a subspace of $H_0^1(\Omega)$ and therefore will be used to discretize the variational formulations previously written. We use in the following P^1 ($l = 1$, piecewise linear) finite elements to approximate the solution and denote $V_h^1 := V_h$.

The finite element approximation of (48) is given as follows: find $\psi_h \in V_h$ such that

$$a(\psi_h, \phi_h) = l(\phi_h), \quad \forall\ \phi_h \in V_h. \tag{68}$$

It is important to observe that the bilinear form in the previous formulation is singular at $r = 0$. This imposes a modification of the polynomial basis functions when a triangle posses a vertex on the axis Oz, as proposed in [12]. An equivalent treatment is applied here, since the quadrature formulas used in FreeFem++ are by default of fifth order and the integrands values are automatically set to zero for vertices on the Oz axis (since we apply here homogeneous Dirichlet boundary conditions $\psi_h = 0$). With this modification, the standard finite element analysis could be applied to our problem (see [12] for details). It is also interesting to note that in FreeFem++ the generic finite-element space W_h^l is a variable type. This allows to switch to P^2 ($l = 2$, piecewise quadratic) finite elements by a simple change of the value of the parameter l, without modifying the rest of the program, and, in particular, the variational formulation.

3.2.1. Convergence of the finite element approximation

We give in the following a convergence result for the finite element discretization using the *natural* norm (15). We first define the standard L^2 projection $P_h : L^2(\Omega) \to V_h$

$$(P_h\psi, \phi_h) = (\psi, \phi_h), \quad \forall\ \phi_h \in V_h, \tag{69}$$

and the following solution operator $L_h : L^2(\Omega) \to V_h$:

$$a(L_h\psi, \phi_h) = L(\phi_h),\ \psi \in H_0(\Omega). \tag{70}$$

In order to give the error estimation, we assume [41,42] that, for a given parameter δ, the triangulation is constructed in such a way that the vortex core boundary ∂S is represented by vertices of the triangulation. A practical technique to generate such meshes is described in Section 4. From (68) and definition (15) we have:

$$\|\psi\|^2 = a(\psi, \psi) = \int_S F\psi\, dx \leqslant \|F\|_{L^2(S)}\|\psi\|_{L^2(S)} \leqslant k(2)|S|^{1/2}\|F\|_{L^2(S)}\|\nabla\psi\|_{L^2(S)}, \tag{71}$$

where $k(2) = 2^{-3/2}$ (see [43]). Using (22), we can further write

$$\|\psi\|^2 \leqslant k(2)\|r\|_{L^\infty(S)}|S|^{1/2}\|F\|_{L^2(S)}\|\psi\|, \tag{72}$$

and, finally,

$$\|\psi\| \leqslant C_F = k(2)\|r\|_{L^\infty(S)}|S|^{1/2}\|F\|_{L^2(S)}. \tag{73}$$

We now define the error $e_h = \psi - L_h\psi$ and infer from (48) and (70) that

$$a(e_h, \phi_h) = 0, \quad \forall \phi_h \in V_h. \tag{74}$$

We have the following error estimation:

$$\|e_h\|^2 = a(e_h, \psi - L_h\psi) = a(e_h, \psi) = a(e_h, \psi - \psi_h) \leqslant \|e_h\|\|\psi - \psi_h\|_{1,2}. \tag{75}$$

Using now the classical (e.g. [43]) H^1 error estimation for P^1 finite elements:

$$\|\psi - \psi_h\|_{1,2} \leqslant Ch\|\psi\|_{H^2(\Omega)}, \tag{76}$$

we finally obtain the standard result:

$$\|e_h\| \leqslant Ch\|\psi\|_{H^2(\Omega)}, \tag{77}$$

with C a constant depending only on Ω.

3.2.2. Convergence of the discrete monotone iterative algorithm

We study in this part the convergence properties of the monotone iterative algorithm at a discrete level. We define a discrete operator for the problem (12)

$$\mathcal{L}_h^* = P_h\mathcal{L}^*. \tag{78}$$

and formulate the discrete iterative algorithm as follows: for any $\phi_h \in V_h$:

- initialize ψ_h^0 by solving the problem (12) for $\delta = 0$:

$$a(\psi_h^0, \phi_h) = (r, \phi_h), \quad \forall \phi_h \in V_h. \tag{79}$$

This solution always exists and is nonzero; it is also the natural starting point for computing the upper solution.

- Compute ψ_h^{n+1} by solving

$$a(\psi_h^{n+1}, \phi_h) = (F(\psi_h^n), \phi_h), \quad \forall \phi_h \in V_h. \tag{80}$$

- stop if $\|\psi_h^{n+1} - \psi_h^n\| / \|\psi_h^{n+1}\| \leqslant \epsilon$, with ϵ fixed.

The proof of the convergence follows the classical methodology [34,37]. We consider only the upper solution, the proof being similar for the lower solution. Let $\psi_u^{0,h} = P_h \psi_u^0$ be the initial condition. Then, the first iteration is:

$$a\left(\psi_u^{1,h}, \phi^h\right) = \left(F(\psi_u^{0,h}), \phi^h\right), \quad \forall \phi^h \in V_h. \tag{81}$$

Since from the finite element approximation of the initial condition $\lim_{h\to 0} \|\psi_u^{0,h} - \psi_u^0\|_{L^2(\Omega)} = 0$, we infer that

$$\lim_{h\to 0} \|F\left(\psi_u^{0,h}\right) - F(\psi_u^0)\|_{L^2(\Omega)} = 0 \tag{82}$$

Since F is discontinuous, the above relation (82) needs some comments since it not stands for all forms of F. In our case, it can be derived by the following short argument: let us denote $\psi_u^0 \in C^2(\overline{\Omega})$ the solution of (12) with $\delta = 0$ and define

$$\Gamma_\delta := \{x \in \Omega : \psi_u^0(x) = \delta\}.$$

According to the convex property of ψ_u^0, $\mathrm{mean}(\Gamma_\delta) = 0$. Thus Γ_δ is a closed curvature. For $\psi_u^{0,h} \in V_h$, we have a similar definition:

$$\Gamma_{\delta,h} := \{\mathbf{x} \in \Omega : \psi_u^{0,h}(\mathbf{x}) = \delta\}, \quad \mathrm{mean}(\Gamma_{\delta,h}) = 0.$$

In our case, $F(\psi) = rI_{\psi \geqslant \delta}$, and we can write

$$\left|F\left(\psi_u^{0,h}\right) - F\left(\psi_u^0\right)\right|_{L^2}^2 = \int_\Omega r^2 \left|I_{\psi_u^{0,h} \geqslant \delta} - I_{\psi_u^0 \geqslant \delta}\right|^2 \mathrm{d}x.$$

We now define the following set

$$\Omega_\delta(\psi) := \{\mathbf{x} \in \Omega : \psi(\mathbf{x}) \geqslant \delta\}.$$

Assuming that $\psi_u^{0,h} \geqslant \psi_u^0$, it is easy to get that

$$\Omega_\delta\left(\psi_u^{0,h}\right) \subset \Omega_\delta\left(\psi_u^0\right).$$

and, consequently,

$$\left|F\left(\psi_u^{0,h}\right) - F\left(\psi_u^0\right)\right|_{L^2}^2 = \int_{\Omega_\delta(\psi_u^{0,h})} r^2 |1-1|^2 \mathrm{d}x + \int_{\Omega_\delta(\psi_u^0)\setminus\Omega_\delta(\psi_u^{0,h})} r^2 |0-1|^2 \mathrm{d}x.$$

Because $|\psi_u^{0,h} - \psi_u^0|_{L^2} \to 0$ as $h \to 0$ and the convexity property,

$$\mathrm{meas}(\Omega_\delta(\psi_u^0) \setminus \Omega_\delta(\psi_u^{0,h})) \to 0, \text{as } h \to 0,$$

which proves (82).

Let us note that the relation (82) means that $\lim_{h\to 0} \|\psi_u^{1,h} - \psi_u^1\| = 0$.

Assuming that $\lim_{h\to 0} \|\psi_u^{n,h} - \psi_u^n\|_{L^2(\Omega)} = 0$, we have

$$\|\psi_u^{n+1,h} - \psi_u^{n+1}\|_{1,2}^2 \leqslant \|\psi_u^{n+1,h} - \psi_u^{n+1}\|^2 = \left(F\left(\psi_u^{n,h}\right) - F\left(\psi_u^n\right), \psi_u^{n+1,h} - \psi_u^{n+1}\right), \tag{83}$$

and, finally,

$$\|\psi_u^{n+1,h} - \psi_u^{n+1}\|_{1,2} \leqslant \|F(\psi_u^{n,h}) - F(\psi_u^n)\|_{L^2(\Omega)}. \tag{84}$$

For a given δ^*, we consider the following two sets

$$\Gamma_{\delta^*}\left(\psi_u^{n,h}\right), \quad \Gamma_{\delta^*}\left(\psi_u^n\right). \tag{85}$$

Since F is a discontinuous function over Ω, we rewrite the right hand side of (84) as following:

$$\begin{aligned}\|F(\psi_u^{n,h}) - F(\psi_u^n)\|_{L^2(\Omega)} &= \|F(\psi_u^{n,h}) - F(\psi_u^n)\|_{L^2(\Omega\setminus(\Gamma_{\delta^*}(\psi_u^{n,h})\cup\Gamma_{\delta^*}(\psi_u^n)))} \\ &\quad + \|F(\psi_u^{n,h}) - F(\psi_u^n)\|_{L^2(\Gamma_{\delta^*}(\psi_u^{n,h})\cup\Gamma_{\delta^*}(\psi_u^n))}.\end{aligned} \tag{86}$$

Due to the continuity of $F(\cdot)$ in the set $\Omega \setminus (\Gamma_{\delta^*}(\psi_u^{n,h}) \cup \Gamma_{\delta^*}(\psi_u^n))$, the first term in the right hand side of (86) goes to 0 when $h \to 0$. At the same time, (12) is strictly convex in $\Omega_{\delta^*}(\cdot)$, and the L-measure $\text{meas}(\Gamma_{\delta^*}(\psi_u^{n,h}))$ and $\text{meas}(\Gamma_{\delta^*}(\psi_u^n))$ are equal to 0. As a consequence, we have

$$\lim_{h\to 0}\|F(\psi_u^{n,h}) - F(\psi_u^n)\|_{L^2(\Omega)} = 0, \tag{87}$$

and, finally,

$$\lim_{h\to 0}\|\psi_u^{n+1,h} - \psi_u^{n+1}\|_{1,2} = 0. \tag{88}$$

Let $\psi_l^{0,h} = P_h\psi_l^0$ be the initial condition for the lower solution. From previous considerations, we have

$$\psi_l^{n,h} \leqslant \psi_l^{n+1,h} \leqslant \cdots \leqslant \psi_u^{n+1,h} \leqslant \psi_u^{n,h}. \tag{89}$$

We can always extract a sub-sequence $\{\psi_u^{n_i,h}\}$ such that this sub-sequence converges strongly in $L^2(\Omega)$ and weakly in $W^{1,2}(\Omega)$ to $\psi_u^{*,h}$. Because of the monotone behavior, the original sequence $\{\psi_u^{n,h}\}$ also converges strongly in $L^2(\Omega)$ and weakly in $W^{1,2}(\Omega)$ to $\psi_u^{*,h}$. Using the triangular inequality

$$\|\psi_u^{n,h} - \psi_u^*\| \leqslant \|\psi_u^{n,h} - \psi_u^{*,h}\| + \|\psi_u^{*,h} - \psi_u^*\|, \tag{90}$$

we easily conclude to the convergence of the discrete solution of the monotone iterative algorithm. The similar results can be obtained for the sequence $\{\psi_l^{n,h}\}$. □

4. Numerical results

The monotone iterative algorithm was implemented in FreeFem++ [29] using P^1 finite elements. The software uses a high level programming language with a syntax close to mathematical formulations making the implementation of the variational formulation (48) straightforward. In all computations we considered the half-domain represented in Fig. 1b, with Dirichlet boundary conditions everywhere, excepting on the axis Or where a Neumann (symmetry) condition is imposed.

The first series of runs considered the (scaled) problem (12) for a fixed geometry ($|OA| = \alpha$ and $|OD| = 1$ in Fig. 1b) and a given value of the parameter δ. We have already displayed in Fig. 2 nonzero solutions for $\alpha = 0.6$. These are obtained using the algorithm for computing the upper solution, since the initial state for $\delta = 0$ always exists and is easy to compute. The field $\psi_u^0(r,z)$ is computing using an initial uniform mesh presented in Fig. 4 a). For subsequent iterations, and, in particular, close to the convergence, we reconstruct the mesh in order to satisfy the assumption made in Section 3.2, assuming that the vortex core ∂S is represented by vertices of the triangulation. This was achieved in practice by extracting the isoline $\psi^n = \delta$ and regenerating the mesh using this line as inner boundary. The advanced automatic mesh generator in FreeFem++ greatly facilitates the implementation of this algorithm. The final mesh (at convergence) is displayed in Fig. 4 b) for a lower resolution that allows to better illustrate this idea.

The iterative algorithm is stopped when the relative change in the solution has a norm lower than $\epsilon = 10^{-6}$. Convergence is very fast, as illustrated in Fig. 5 by plots of the evolution of the maximum of the solution ψ_{max}^n and the energy η given by (35). We observe that convergence is faster for lower values of δ, which is not surprising since low values of delta represent larger vortex cores and, consequently, a better discretization of this region. For values of δ close to δ_{max}, more iterations are needed, but always lower that one hundred. This proves that our algorithm is much faster than the method of Durst et al.

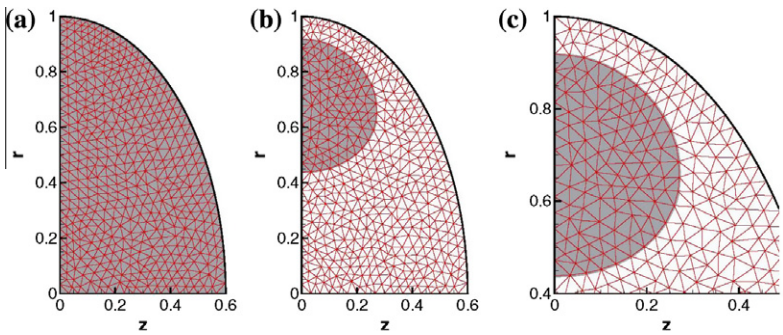

Fig. 4. Solutions for the elliptic vortex with $\alpha = 0.6, \delta^{-1} = 154$. Illustration of the initial mesh (a) and final mesh (b) with accurate capture of the vortex core boundary ∂S. (c) Final mesh, zoom in the region of the vortex core represented by gray patches.

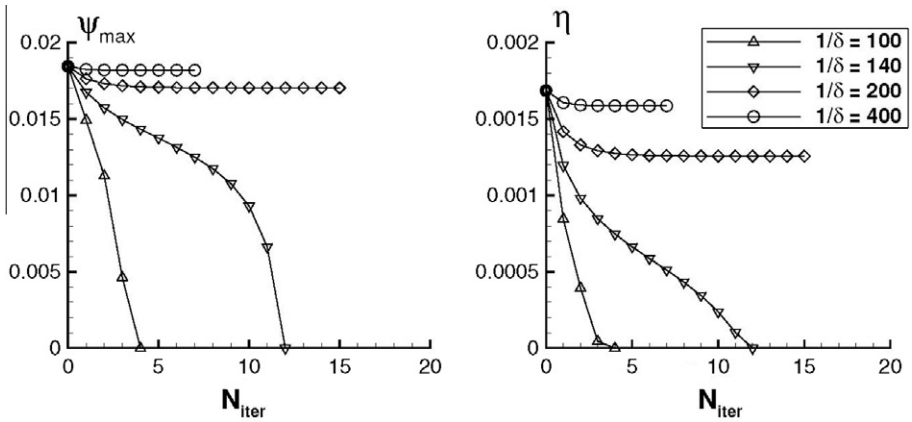

Fig. 5. Solutions for the elliptic vortex with $\alpha = 0.6$. Convergence history tracking the maximum of the solution (ψ_{max}) and energy $\eta = a(\psi, \psi)$.

[9,10] using finite differences for the same problem; according to their convergence reports, several thousands of iterations were needed to reach the converged solution.

A second series of runs was devoted to the numerical estimation of the critical parameter δ_{max} for which nonzero solutions still exist. The monotone iterative algorithm was embedded into a dichotomy algorithm refining the value of δ_{max} up to 6 digits; we used a refined mesh with $h(\mathcal{T}_h) = 0.01$, where

$$h(\mathcal{T}_h) = \max\{\mathrm{diam}(T_k) | T_k \in \mathcal{T}_h\}, \quad \mathrm{diam}(T_k) = \sup_{(x,y)\in T_k} |x - y|. \tag{91}$$

Computed values are plotted in Fig. 3 showing a good agreement with data reported by Durst et al. [9,10]. The numerical values for δ_{max} are compared in the same figure with theoretical estimations derived in Section 2. For both theoretical estimations, the eigenvalues of the elliptic operator $\mathcal{L}$ on the elliptic domain are computed using the shift–invert mode method implemented in ARPACK library. The values are carefully checked and for the refined mesh, the definition relationship (18) is verified up to double precision (10^{-12}).

It is interesting to note that the dichotomy algorithm computing δ_{max} is initialized considering the search interval $[0, \psi^0_{max}/2]$, where ψ^0 is the solution obtained for $\delta = 0$. This is an obvious choice, but time consuming. A refined initial guess using the second theoretical estimation (Proposition 2) for δ_{max} results in a considerable computational time reduction. This observation could be useful in practical applications searching for the admissible vortex ring solution with a minimal vortex core area.

We finally discuss computations dealing with upper and lower solutions. This particular behavior of numerical algorithms is due to the discontinuity of the vorticity function F and was not previously addressed in numerical studies of vortex rings. From a practical viewpoint, we emphasize the fact that different solutions could be obtained when starting from different

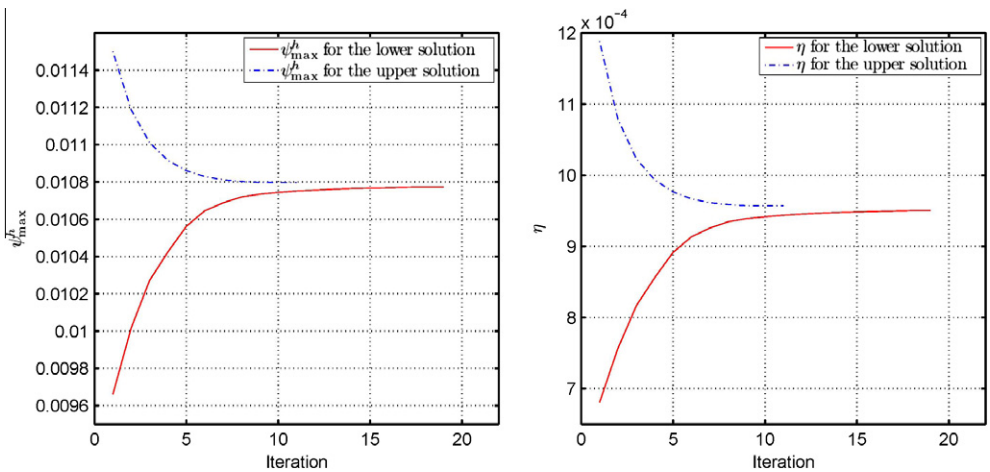

Fig. 6. Upper and lower solutions for the elliptic vortex with $\alpha = 0.6$. Evolution of ψ_{max} and energy during the iterative computation. Mesh resolution $h(\mathcal{T}_h) = 0.02$.

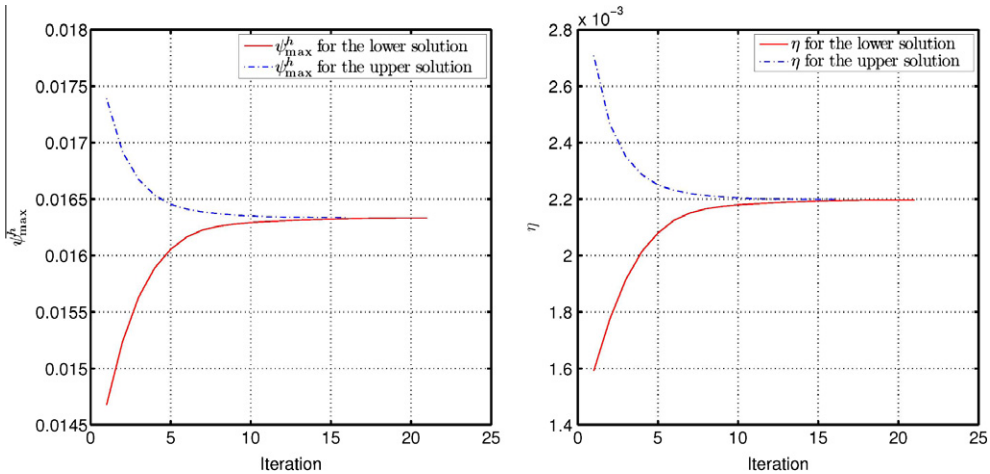

Fig. 7. Upper and lower solutions for the elliptic vortex with $\alpha = 0.6$. Evolution of ψ_{max} and energy during the iterative computation. Mesh resolution $h(\mathcal{T}_h) = 0.01$.

initial conditions. This property that we have theoretically addressed in Section 2 is visible in computations, and in particular for less refined grids, that are usually employed in practical computations involving complex fluid flow interactions.

We consider again the elliptical domain with $\alpha = 0.6$ and compute the solution for $\delta = 1/176$. For this geometry, the computed critical value is $\delta_{max} = 1/153.28$. The upper solution is computed using as initial condition the solution obtained for $\delta = 0$ (with highest possible energy), while the lower solution algorithm starts from the solution with $\delta = 1/153.62$. The convergence tolerance ϵ is fixed to 10^{-6}.

In Fig. 6 we monitor the evolution of the maximum of the solution and the corresponding energy along the iterative process. The mesh size is $h(\mathcal{T}_h) = 0.02$, which is a reasonable resolution for practical applications (for reference, 50 grid points are placed on the border *OD* in Fig. 1b and the mesh is generated with quasi-constant h). We notice that, although the same convergence tolerance is imposed, final values are different for the lower and the upper solution. As a consequence, the calculation of basic quantities of practical interest (energy, vortex core area, translation velocity) results in different values depending whether the upper or lower solution is considered.

When the mesh is refined, the difference between the upper and lower solution becomes negligible, as shown in Fig. 7 for a mesh size $h(\mathcal{T}_h) = 0.01$. This suggests that the mesh size has to be carefully set in practical calculations, considering not only the classical analysis of the finite element approximation, but also the dependence of the converged solution on the initial condition.

A final important result is provided by the plots in Fig. 8 showing solution profiles along the radial axis *Or*. When the solution is normalized with its maximum value, we obtain the collapse of all profiles, for all geometrical aspect ratios α. This

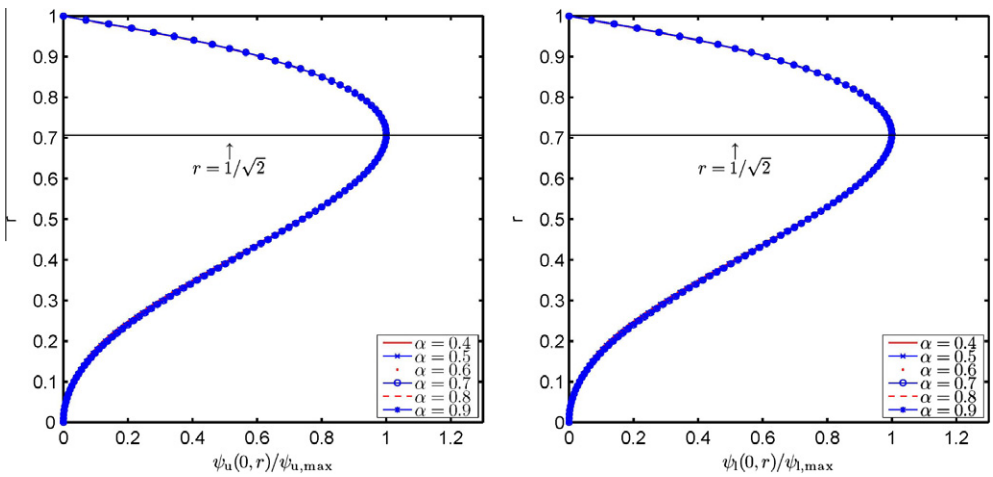

Fig. 8. Upper and lower solutions for the elliptic vortex with different aspect ratios α. Solution profiles along the *Or* axis. The vortex core corresponds to $\delta = \delta_{max}$ for all computations.

observation stands for both upper and lower solutions (the mesh size is $h(\mathcal{T}_h) = 0.01$ for all cases). The maximum of ψ/ψ_{max} is reached at approximately $r = 1/\sqrt{2}$, which is the value corresponding to the center of the Hill's spherical vortex. This result, which is also reported in [10], strongly supports the assumption made in Section 2 for the approximation of geometrical quantities characterizing the vortex ring core.

5. Summary and future work

We developed in this paper a new algorithm to compute vortex rings solutions in stationary ideal flows. The boundary separating the vortex ring from the external (potential) flow is assumed of elliptic shape. The difficulty of the problem consists in the fact that the source term depends on the solution itself through a discontinuous function. The algorithm is based on the monotone iterative calculation of the solution and takes into account the discontinuity of the source term by considering separately the upper and lower solution [32,34,36,37]. We theoretically prove the convergence of the algorithm in a general framework, and in the particular setting using finite elements for the spatial discretization.

The algorithm was implemented using the free software FreeFem++ [29] and proved very efficient to compute vortex ring solutions. Convergence is considerably faster than that reported in previous studies [9,10]. Numerical computations allowed to point out the differences between the upper and lower solutions, which is, to the best of our knowledge, a novelty in this investigation field. Direct consequences of this behavior for practical computations were also emphasized.

We also derived a refined analytical estimation of the critical parameter for the existence of nonzero solutions. This theoretical prediction is fairly well supported by numerical results and could be very useful for practical applications. One of such applications concerns the fuel injection in automotive engines. The impulsive start of the flow generates large recirculating zones that are not accessible to usual measurements by PIV (Particle Image Velocimetry) because of the concentration of a large number of fuel droplets. Since these recirculation zones are well described by vortex rings models, the missing velocity field from experiments could be reconstructed by the theoretical model considered in this paper. In particular, the theoretical estimation of the critical parameter could be used to investigate admissible solutions, while the fast algorithm designed in this study could be the basis of a real-time reconstruction of the velocity field. These topics are related to the field reconstruction problems for Tokamak plasma reactors [44].

Acknowledgement

We acknowledge very useful and stimulating discussions with Nam Q. Le and Sylvia Serfaty on the theoretical estimation of critical parameters. This work has been supported by the Programme MAGIE-FUI7 Pôle MOVEO.

References

[1] K. Mohseni, A formulation for calculating the translational velocity of a vortex ring or pair, Bioinspirat. Biomimet. 1 (2006) S57–S64.
[2] J.O. Dabiri, Optimal vortex formation as a unifying principle in biological propulsion, Ann. Rev. Fluid Mech. 41 (1) (2009) 17–33.
[3] S. Begg, F. Kaplanski, S. Sazhin, M. Hindle, M. Heikal, Vortex ring-like structures in gasoline fuel sprays under cold-start conditions, Int. J. Engine Res. 10 (4) (2009) 195–214.
[4] F. Kaplanski, S.S. Sazhin, S. Begg, Y. Fukumoto, M. Heikal, Dynamics of vortex rings and spray-induced vortex ring-like structures, Eur. J. Mech. B/Fluids 29 (3) (2010) 208–216.
[5] I. Danaila, J. Hélie, Numerical simulation of the postformation evolution of a laminar vortex ring, Phys. Fluids 20 (2008) 073602.
[6] J. Norbury, A family of steady vortex rings, J. Fluid Mech. 57 (1973) 417–431.
[7] L.E. Fraenkel, Examples of steady vortex rings of small cross-section in an ideal fluid, J. Fluid Mech. 51 (1972) 119.
[8] F.B. Kaplanski, Y.A. Rudi, A model for the formation of optimal vortex ring taking into account viscosity, Phys. Fluids 17 (2005) 087101.
[9] F. Durst, B. Schönung, M. Simons, Steady ellipsoidal vortex rings with finite cores, J. Appl. Math. Phys. (ZAMP) 32 (1981) 156–169.
[10] F. Durst, B. Schönung, Computations of steady, ellipsoidal vortex rings with finite cores, Comput. Fluids 10 (1982) 87–93.
[11] L.E. Fraenkel, M.S. Berger, A global theory of steady vortex rings in an ideal fluid, Acta Math. 132 (1974) 13–51.
[12] H. Berestycki, E. Fernandez Cara, R. Glowinski, A numerical study of some questions in vortex ring theory, RAIRO Anal. Num. 18 (1984) 7–85.
[13] W.M. Ni, On the existence of global vortex rings, J. d'Anal. Math. 37 (1980) 208–247.
[14] A. Ambrosetti, M. Struwe, Existence of steady vortex rings in an ideal fluid, Arch. Rational Mech. Anal. 108 (2) (1989) 97–109.
[15] M.J. Esteban, Nonlinear elliptic problems in strip-like domains: symmetry of positive vortex rings, Nonlinear Anal. Theory Methods Appl. 7 (1983) 365–379.
[16] Tadie, On the bifurcation of steady vortex rings from a Green function. Math. Proc. Camb. Phil. Soc. 116 (1994) 555–568.
[17] I. Danaila, C. Vadean, S. Danaila, Specified discharge velocity models for the numerical simulation of laminar vortex rings, Theor. Comput. Fluid Dyn. 23 (2009) 317–332.
[18] M.J.M. Hill, On a spherical vortex, Philos. Trans. Roy. Soc. Lond. A185 (1894) 213–245.
[19] H. Lamb, Hydrodynamics, Dover, New York, 1932.
[20] G.K. Batchelor, An Introduction to Fluid Dynamics, seventh ed., Cambridge University Press, Cambridge, NY, 1988.
[21] C.J. Amick, L.E. Fraenkel, The uniqueness of a family of vortex rings. Arch. Rational Mech. Anal. (1988) 207–241.
[22] C.J. Amick, L.E. Fraenkel, The uniqueness of Hill's spherical vortex, Arch. Rational Mech. Anal. 92 (1986) 91–119.
[23] J. Norbury, A steady vortex ring close to Hill's spherical vortex, Proc. Cambridge Phil. Soc. 72 (1972) 253–282.
[24] L.E. Fraenkel, A lower bound for electrostatic capacity in the plane, Proc. Roy. Soc. Edinburgh A88 (1981) 267–273.
[25] Tadie, Problèmes elliptiques à frontière libre axi-symétriques: estimation du diamètre de la section au moyen de la capacité. Potential Analysis 5 (1996) 61–72.
[26] L. Fraenkel, A lower bound for electrostatic capacity in the plane, Proc. Roy. Soc. Edinburgh Sect. 88 (3–4) (1981) 268–273.
[27] N.Q. Le, Private Communication, 2008.
[28] N.Q. Le, Regularity and nonexistence results for some free-interface problems related to Ginzburg–Landau vortices, Interfaces and Free Boundaries 11 (2009) 139–152.
[29] F. Hecht, O. Pironneau, A. Le Hyaric, K. Ohtsuke, FreeFem++ (manual), <www.freefem.org>, 2007.

[30] I. Danaila, P. Kazemi, A new Sobolev gradient method for direct minimization of the Gross-Pitaevskii energy with rotation, SIAM J. Sci. Comput. 32 (2010) 2447–2467.
[31] I. Danaila, F. Hecht, A finite element method with mesh adaptivity for computing vortex states in fast-rotating Bose–Einstein condensates, J. Comput. Phys. 229 (2010) 6946–6960.
[32] S. Carl, S. Heikkilä, Fixed Point Theory in Ordered Sets and Applications, Springer-Verlag, New York, 2011.
[33] S. Carl, S. Heikkilä, On extremal solutions of an elliptic boundary value problems involving discontinuous nonlinearities, Diff. Integr. Equat. 5 (1992) 581–589.
[34] S. Carl, C. Grossmann, Boundary value problems with discontinuities and monotone discretization, J. Comput. Appl. Math. 51 (1994) 293–303.
[35] S. Carl, S. Heikkilä, Extremal solutions of quasilinear parabolic boundary value problems with discontinuous nonlinearities, Dyn. Syst. Appl. 3 (1994) 251–258.
[36] Y. Zhang, Monotone convergence of finite element approximations of obstacle problems, Appl. Math. Lett. 20 (2007) 445–449.
[37] Q. Zou, Monotone iteration for elliptic pdes with discontinuous nonlinear terms, Numer. Math. 14 (4) (2005) 363–374.
[38] L.C. Evans, Partial Differential Equations, American Mathematical Society, 2010.
[39] R. Adams, Sobolev Spaces, Academic Press, New York, 2003.
[40] P.G. Ciarlet, The finite element method for elliptic problems, Studies in Mathematics and its Applications, Amsterdam, North-Holland, 1978.
[41] R. Glowinski, Numerical Methods for Nonlinear Variational Problems, Springer-Verlag, Berlin and Heidelberg, 2008.
[42] R.K. Sinha, B. Deka, Finite element methods for semilinear elliptic and parabolic interface problems, Appl. Numer. Math. 59 (8) (2009) 1870–1883.
[43] A. Quarteroni, A. Valli, Numerical Approximation of Partial Differential Equations, Springer-Verlag, Berlin and Heidelberg, 1994.
[44] J. Blum, C. Boulbe, B. Faugeras, Real time reconstruction of plasma equilibrium in a tokamak, International Conference on Burning Plasma Diagnostics, Villa Monastero, Varenna, 2007.